Journal of Nuclear Materials 545 (2021) 152618

Contents lists available at ScienceDirect

Journal of Nuclear Materials

journal homepage: www.elsevier.com/locate/jnucmat

Crystallization behavior and mechanical response of metallic glass induced by ion irradiation at elevated temperature

Kun Zhang[a,d], Yang Wang[a,d], Wanhao Zhang[c], Zheng Hu[c], Bingchen Wei[a,b,d,*], Yihui Feng[d,e]

[a] CAS Key Laboratory of Microgravity (National Microgravity Laboratory), Institute of Mechanics, Chinese Academy of Sciences, Beijing 100190, China
[b] Center of Materials Science and Optoelectronics Engineering, University of Chinese Academy of Sciences, Beijing 100049, China
[c] Science and Technology on Vehicle Transmission Laboratory, China North Vehicle Research Institute, Beijing 100072, China
[d] School of Engineering Science, University of Chinese Academy of Sciences, Beijing 100049, China
[e] State Key Laboratory of Nonlinear Mechanics, Institute of Mechanics, Chinese Academy of Sciences, Beijing 100190, China

ARTICLE INFO

Article history:
Received 28 June 2020
Revised 16 September 2020
Accepted 19 October 2020
Available online 24 October 2020

Keywords:
metallic glass
ion irradiation
crystallization
mechanical properties
nanoindentation

ABSTRACT

When exposed to heavy-ion radiation, metallic glasses (MGs) often exhibit an excellent irradiation tolerance at room temperature compared with their crystalline counterparts; however, their structural evolution and mechanical response at elevated temperature is largely unknown. Here, the phase stability and crystallization behavior of ZrTiHfCuBeNi MG were investigated by irradiating it with an 8.0 MeV Xe^{29+} ion beam at 550°C. Nanocrystal precipitation randomly appeared in the MG matrix at low fluences, which overlapped and aggregated at higher fluences. In addition, non-edge-on faulted dislocations were formed between neighboring grains due to irradiation-induced stress. Moreover, delays in the first pop-in events after irradiation were attributed to irradiation-induced structural rearrangement and the precipitation of nanocrystals. This work sheds light on the structural evolution and mechanical properties of MGs when irradiated at elevated temperature.

1. Introduction

Metallic glasses (MGs) have been the focus of much recent research because of their unique mechanical and chemical properties [1-3], such as a high yield strength, large elastic deformation, and outstanding corrosion and wear resistance [4-10]. Their response to radiation is also significantly different from crystalline solids due to the lack of self-interstitials, vacancy loops, and grain boundaries. Their structure also affects their material properties during irradiation, especially as it relates to the mechanical behavior of MGs [11-14]. For instance, crystalline solids may undergo unlimited swelling under continuous irradiation, while MGs only expand and contract following irradiation at room temperature [15,16]. Irradiation generally embrittles crystalline solids, but some irradiated MGs become more ductile and retain their fully amorphous state at irradiation temperature far from the glass transition temperature (T_g) [17]. This occurs because pairs of free volume-like defects and their counterparts are formed by the displacement of a single atom in localized regions, and these “defects” can be homogenized or annihilated in MGs [18,19]. In a word, MGs are considered to be ideal candidates for applications in nuclear-irradiated environments at room temperature.

Since actual irradiation conditions in fission or fusion reactors are accompanied by high temperature, only a few studies have investigated the phase stability and crystallization behaviors of MGs after irradiation at elevated temperature [20]. Free-volume models have shown that ion irradiation can significantly affect the nucleation and crystallization processes of MGs by increasing the short-range atomic mobility. However, thermal spikes during ion-solid interactions may not be the main cause of nanocrystal formation because the cooling rate is several magnitudes higher than the critical cooling rate required for amorphous phase formation. Shao et al. also found that the temperature required for nanocrystal formation is notably lower than the T_g in MGs [21]. It is generally believed that crystallization phenomena are associated with thermal activation. For many types of MGs, the nucleation barrier is usually slightly lower than the energy barrier of nanocrystal growth [8]. If the temperature is high enough to overcome this nucleation barrier, dramatic growth can also occur, however, the mechanism of crystallization induced by irradiation at elevated temperature is still unknown.

It is imperative to explore the microstructure evolution, as well as the correlation between structure heterogeneity and nanocrystal growth to further clarify the influence of irradiation on MGs at

* Corresponding author.
E-mail address: weibc@imech.ac.cn (B. Wei).

https://doi.org/10.1016/j.jnucmat.2020.152618
0022-3115/

elevated temperature. In this study, we investigate the effect of Xe^{29+} ion irradiation at 550 °C on the structural and mechanical properties of ZrTiHfCuBeNi MGs. As a new high-entropy metallic glass (HE-MG), the alloy combines both the advantages of high-entropy alloys and MGs, is believed to an excellent irradiation tolerance material in nuclear fields [22]. The mechanical behaviors after irradiation were also investigated. This work provides an opportunity to shed light on the structural evolution and mechanical mechanism of MGs at elevated temperature irradiation.

2. Materials and Methods

Vacuum suction casting was used to produce ZrTiHfCuBeNi MG rods with a diameter of 5 mm. The raw materials used for the alloy had a purity of 99.99%. Wafer samples with 2.0 mm in thickness were cut from the resulting rods. Prior to irradiation experiments, the surfaces of samples were polished using 600, 1200, 2000 and 3000 grit SiC paper successively, then they were polished to a mirror finish with 40 nm SiO_2. Irradiation experiments were conducted at 550 °C with 8.0 MeV Xe^{29+} using a 320 kV multi-discipline research platform for highly-charged ions (Institute of Modern Physics, Chinese Academy of Sciences, Lanzhou, China), at a pressure near or below 10^{-5} torr.

The depth distribution of implanted Xe^{29+} ions and irradiation damage (displacement per atom, dpa) were simulated using the Ion Distribution and Quick Calculation of Damage modes in SRIM-2008 software [23]. The SRIM simulations of 8.0 MeV Xe^{29+} radiation into the MG indicated maximum damage values of approximately 0.4 dpa and 2.0 dpa after irradiation with 1×10^{14} ions/cm^2 and 5×10^{14} ions/cm^2, respectively, as indicated by the white line in Fig. 1(a) and (b).

The microstructures were characterized by X-ray diffraction (XRD, Philips PW 1050 diffractometer with Cu-Kα radiation, Amsterdam, Netherlands) operating at 45 keV, a 0.01 step size, and a 200 mA current for phase analysis with improved accuracy. The size of the diffraction area on the metallic glass surface was 0.5 mm, with a scanning speed of 2°/min. Each sample was examined three times in different areas. The microstructures of samples were also analyzed by a transmission electron microscope (TEM, FEI Tecnai G^2 F20, Tokyo, Japan). Focused ion beam (FIB, Helios Nanolab 600) was used to prepare pristine and irradiated samples for TEM observation. TEM and high-resolution TEM (HRTEM) were operated at 200 kV. To investigate the microstructural evolution of MGs induced by ion irradiation, nanoindentation experiments were conducted on pristine and irradiated samples using an Agilent Technologies Nano Indenter G200, equipped with a Berkovich diamond indenter at 20°C, after calibration on standard fused silicon. The loading rate was 0.05 mN/s, with a maximum loading of 20 mN. To remove thermal effects, the thermal drift of the instrument was maintained below 0.05 nm/s. Each sample was subjected to 20 trials over a space wider than 50 μm.

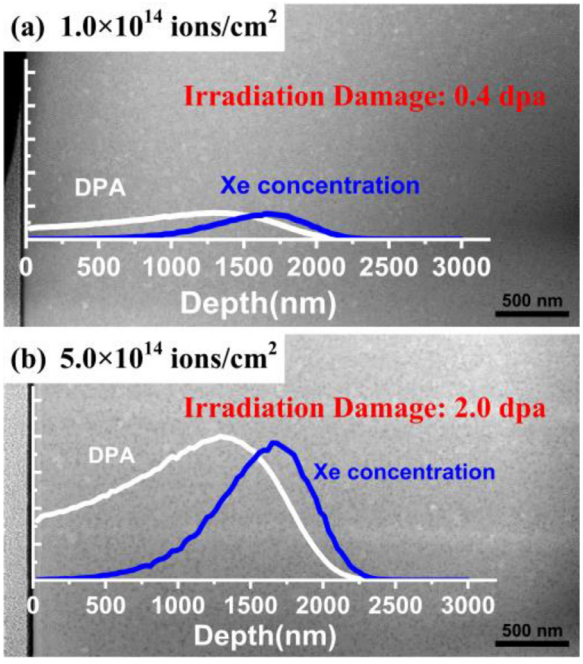

Fig. 1. Depth profile of irradiation damage and implanted ion concentration in ZrTiHfCuBeNi MG irradiated by 8.0 MeV Xe^{29+} at (a) 1×10^{14} ions/cm^2 and (b) 5×10^{14} ions/cm^2, respectively, calculated by SRIM-2008 (quick mode). The back-grounds are TEM-BF images with the above mentioned irradiation dosage.

3. Results and discussion

3.1. Microstructure characterization

Fig. 2(a) shows the DSC traces of the pristine samples of ZrTiHfCuBeNi MG at a constant heating rate of 20 K/min, scanned from RT to 550°C. The glass transition temperature (T_g) and crystallization temperature (T_x) of the samples are indicated by arrows. The T_g and T_x of ZrTiHfCuBeNi MG were 410 °C and 460°C.

The XRD patterns of the pristine and irradiated samples are shown in Fig. 2(b). The pristine MG sample showed only a typical broad halo peak near 2θ=38°, and no sharp diffraction peaks corresponding to a crystalline structure were observed. After ion irradiation, diffraction peaks appeared and overlapped with the broad amorphous peak, suggesting that the MG microstructure changed after Xe irradiation. As marked in Fig. 2(b), the crystalline products at different stages were a face-centered cubic (fcc) solid solution, a small amount of body-centered cubic (bcc) solid solution, and some intermetallic compounds (IMCs) (e.g., Ni_7Zr_2) [24,25]. As the fluence increased, the diffraction peaks became more defined and sharper, suggesting the development of a more ordered structure. Yang et al. [26] have reported that an MG with a similar composition, ZrTiHfCuBe, exhibited a broad halo that overlapped with a few crystalline peaks on its XRD pattern at 799 K (526°C, which is near the irradiation temperature in this study). This indicated that the specimen still contained a large portion of an amorphous structure. In this study, crystallization peaks were already apparent after Xe irradiation at a similar temperature, suggesting the nanoparticle growth process was even faster than in an MG subjected to annealing. The dissociative atoms created by ion irradiation may exist due to thermal excitation under ion irradiation at 550°C, and ion irradiation-induced interstitial atoms may also increase atomic migration and nanoparticle growth.

The microstructure of the irradiated MGs was further studied by TEM. Fig. 3(a) and (c) show the TEM bright-field profiles of irradiated samples prepared by FIB with 0.4 dpa and 2.0 dpa, respectively. Fig. 3(b) and (d) show the TEM bright-field images of the irradiated regions at high magnifications. The corresponding selected area electron diffraction (SAED) patterns, as well as the crystalline nanoparticle distributions, are shown in the inset. Nanoparticle precipitation occurred in MGs subjected to Xe irradiation, with 0.4 dpa and 2.0 dpa at 550°C. The SAED pattern in the inset contains some discontinuous Debye rings and numerous sharp diffraction spots on the halos, confirming the crystalline nature of the irradiated MGs, in agreement with the XRD patterns. Upon further ion irradiation up to 2.0 dpa, the intensities of the diffraction spots and discontinuous Debye rings increased. This was accompanied by a weakening of the halo rings, and the granular contrast image became sharper, showing that the number of precipitates increased [18]. Moreover, the average nanoparticle diameter, $\bar{d}$, in ir-

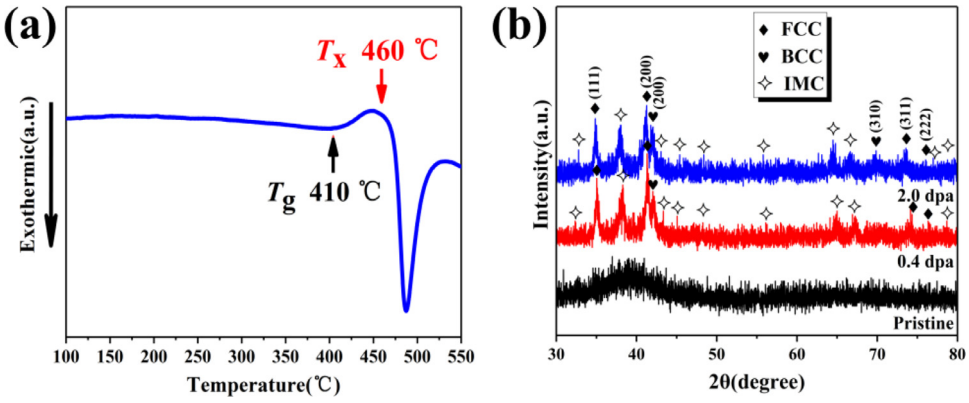

Fig. 2. (a) The DSC curves of pristine ZrTiHfCuBeNi MG at a heating rate of 20 K/min and (b) XRD patterns of pristine and irradiated ZrTiHfCuBeNi MGs.

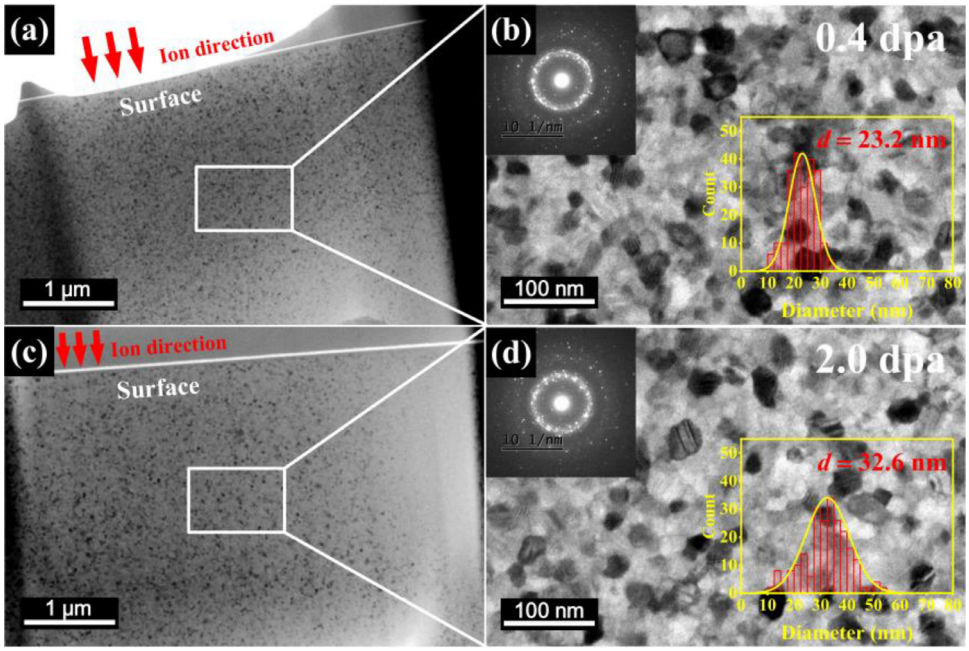

Fig. 3. The cross-sectional bright-field images of MGs irradiated at different dosage (a) 0.4 and (c) 2.0 dpa. The magnified morphology of the nanocrystal size is presented in Fig (b) and (d). the corresponding selected area electron diffraction (SAED) patterns and nanoparticle distribution are exhibited in the insets.

radiated MGs with 0.4 dpa and 2.0 dpa were measured to be 23.2 nm and 32.6 nm, according to the bright-field TEM images, respectively. The region within the projected range and beyond the projected range at 2.0 dpa has been applied in supplementary materials, some nanoparticles were formed and homogeneously dispersed in the amorphous matrix in the region beyond the projected range, which is entirely different from the region within the projected range. In addition, the average nanoparticle diameter beyond the projected range were measured to be 26.2 nm, which is slightly smaller than the one in the region within the projected range (32.6nm). Moreover, the interface between nanocrystals and glassy matrix is not clear within the projected range. That means, the ion irradiation at the elevated temperature can significantly accelerate the crystallization of MGs with the combined effect of the irradiation and thermal annealing [20, 27].

HRTEM was used to further characterize the crystalline nanoparticles. Fig. 4(b) and (d) show the HRTEM images of irradiated MGs with 0.4 dpa and 2.0 dpa, selected from the bright-field images (Fig. 4(a) and (b)), respectively. The corresponding Fourier transform (FT) pattern obtained from the red square area is exhibited in the inset. When the irradiation damage was 0.4 dpa, some nanoparticles were formed and were homogeneously dispersed in the amorphous matrix, as shown in Fig. 4(a) and (b). The crystalline nanoparticles were identified as FCC phase by FT, suggesting that it was the major phase and was preferentially formed, along with other nucleating phases with complicated structures under Xe irradiation at 550°C. According to Fig. 4(a) and (c), the estimated crystallization rates per unit area were about 36% and 73% at 0.4 and 2.0 dpa, respectively. The metastable structure of MGs can change due to atomic vibrations when the temperature fluctuates. In particular, when the temperature reaches T_g, atom diffusion intensifies, and the energy of the system will transition from a metastable state to a stable state, and the MG will crystallize. However, when the fluence increased, the crystallization behavior was further intensified, and the precipitated nanoparticles began to overlap, as shown in Fig. 4(c).

Generally, the irradiation can induce stress concentration around precipitated nanoparticles and bring a lot of defects. The results show that although the elevated temperature ion irradiation would not introduce observable structural defects in metallic glass, the excess free volume induced by ion irradiation would promote the formation of nanocrystals under thermal annealing. Most of the defects produced by displacement cascade may recombine and annihilate in the boundary between the existed precipi-

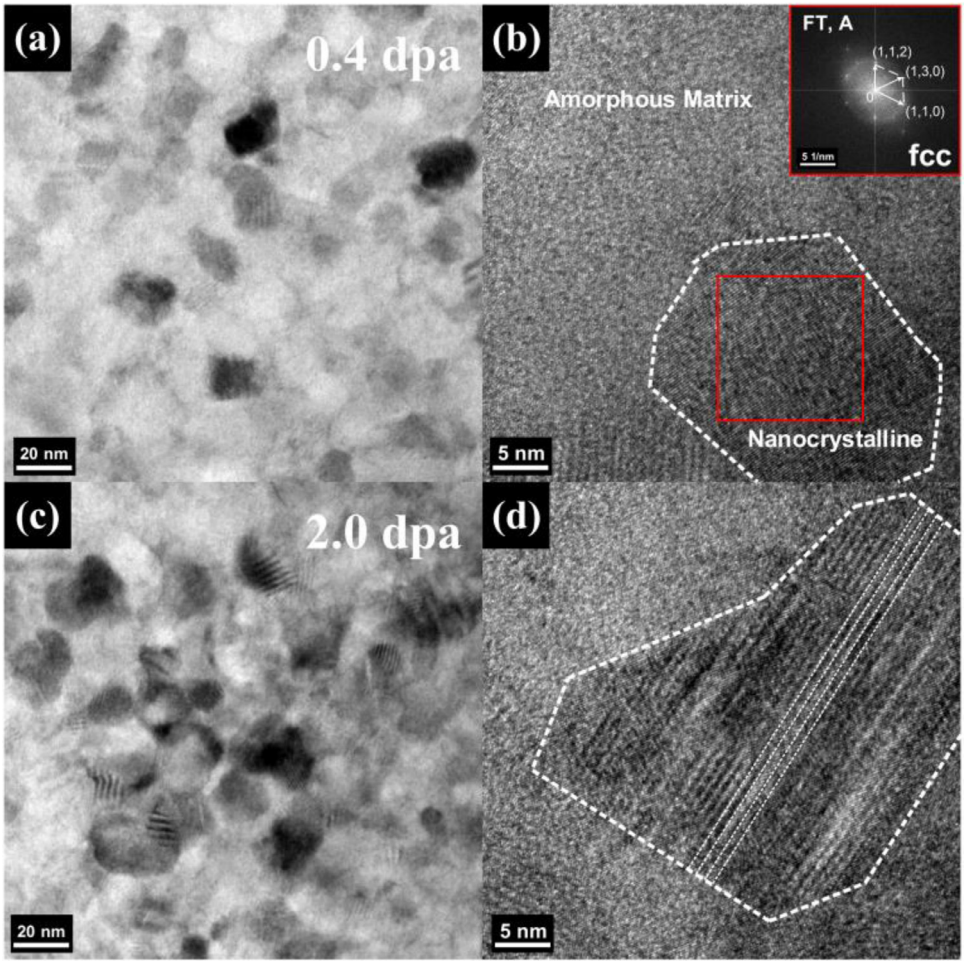

Fig. 4. HRTEM images of irradiated MGs at different dosage: (a) 0.4 and (c) 2.0 dpa. The corresponding magnified morphologies of the nanocrystal are presented in Fig. (b) and (d), repetitively.

tated nanoparticles and the amorphous matrix, which may serve as a new nucleation for subsequent crystallization [26]. Moreover, some defects, such as the non-edge-on faulted dislocations, were formed through the nanoparticles at 2.0 dpa, as shown in Fig. 4(d). The visible parallel fringes (marked by the white dotted line) are a signature of stacking faults, and the underlying mechanism during Xe irradiation is closely related to the evolution of point defects. The appearance of the stacking faults may be dependent on the crystalline species, which usually appeared in the multicomponent alloy with a large difference in atomic size. During irradiation, most of the Frenkel pairs produced by energetic displacement cascade could recombine and annihilate, whereas the residual point defects (vacancies and interstitials) could diffuse and evolve into defects with different geometrical configurations and energy states [27, 28]. In this work, to reduce system energy at a higher fluence, interstitials coalesced and precipitated into defects, e.g., non-edge-on faulted dislocations. Thus, ion irradiation not only accelerated the atomic migration and growth of nanoparticles, but also caused lattice distortion defects in the formed nanoparticles [26].

3.2. Mechanical behavior

Nanoindentation is an effective technique for characterizing the nanomechanical behavior of quasi-brittle materials like MGs under a reasonably well-defined stress state [29,30]. Fig. 5(a-c) show the representative load-displacement (*P-h*) curves obtained from nanoindentation tests at a constant loading rate of 0.05 mN/s and a maximum load of 20 mN. The pristine sample showed a serrated flow or pop-in phenomenon, which manifested as a sudden indentation displacement during the loading process of the nanoindentation tests, as shown in Fig. 5(a). However, the increased fluence substantially changed the nature of the serration events, from the ideal stair-step-like *P-h* curves in the pristine sample, to the ripple-shaped (or even smooth) parabolic curves of the irradiated samples as the fluence increased, as shown in Fig. 5(b) and (c). Meanwhile, the number of pop-in events in the *P-h* curves—which indicated the onset of plasticity—dramatically decreased as the fluence increased. For MGs, the pop-in events corresponded to the activation of individual shear events [31-33]. Crystalline materials have been proposed as a link to homogeneous dislocation nucleation or the activation of a defect source such as dislocations, vacancies, or stacking faults [34-37]. In this present study, upon increasing the irradiation fluence at high temperature, the MGs changed from a glassy to a crystalline state, and the pop-in phenomenon gradually decreased.

For an accurate analysis, we identified the pop-in events [38]. The displacement versus time (*h-t*) curve was differentiated by a two-point forward-derivative algorithm to obtain a curve of velocity versus time (d*h*/d*t*-*t*), as depicted in Fig. 5(d-f). As shown in Fig. 5(d), for the pristine sample, the pop-in events corresponding to the sharp bursts on the d*h*/d*t*-*t* curve appeared, along with many fluctuations with higher frequencies but smaller amplitudes that were related to the instrument noise. At 0.4 dpa after Xe irradiation, as shown in Fig. 5(e), the number of sharp bursts de-

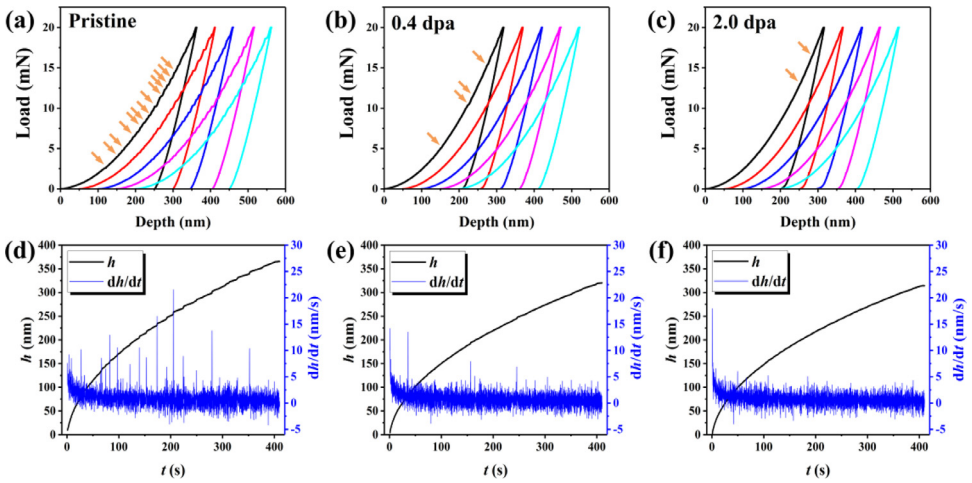

Fig. 5. Representative load-displacement (*P*-*h*) curves of ZrTiHfCuBeNi MG at irradiation damages of (a) 0, (b) 0.4 dpa, and (c) 2.0 dpa (the arrow points to the pop-in events); the displacement versus time (*h*-*t*) curves and their corresponding time derivative of displacement versus time (d*h*/d*t*-*t*) at irradiation damages of (d) 0, (e) 0.4 dpa, and (f) 2.0 dpa. The loading rate was constant at 0.05 mN/s during nanoindentation tests.

Table 1
The mean values of nanohardness (H), Young's modulus (E), and indent load at the first pop-in event (P_c) of the pristine and irradiated ZrTiHfCuBeNi MGs.

Sample	$\bar{H}$, GPa	$\bar{E}$, GPa	$\bar{P}_c$, mN
Pristine	9.79	145.17	0.89
0.4 dpa	12.78	181.09	4.75
2.0 dpa	13.24	187.33	11.11

creased significantly. Here, the pop-in events represent the localized inhomogeneous plastic flow of the MGs under loading, and weaker serrations indicated a better plastic deformation capacity. The intensity of pop-in events can be tuned by applying a different indentation rate, where a slower indentation rate promotes more serrations, and a faster indentation suppresses pop-in events. Here, the loading rates of the samples with different fluences were constant. Thus, the weakening of the pop-in events after Xe irradiation at 550 °C was attributed to crystallization, accompanied by an improvement in the plasticity of irradiated MGs. Interestingly, with irradiation damage up to 2.0 dpa, the sharp bursts almost disappeared during loading.

The average nanohardness (H), Young's modulus (E), and indent load at the first pop-in event (P_c) of the pristine and irradiated MGs were measured by nanoindentation tests, as shown in Table 1. A clear trend can be observed in which the nanohardness and modulus of the MGs increased gradually upon increasing the irradiation fluence. The improved hardness of the irradiated MGs occurred due to the formation of nanoparticles, which hindered the appearance of the shear motions. The Young's modulus was improved due to the nanostructured precipitates, which affected the interatomic distances of the MGs [26]. Moreover, the mean values of the applied load corresponding to the first pop-in events, $\bar{P}_c$, were determined to be 0.89, 4.75, and 11.11 mN for the pristine and irradiated MGs, respectively. This indicates that the first pop-in events began to gradually lag as the fluence increased.

In a thermal-mechanical coupled framework, the activation of the shear transformation of MGs underneath the indenter may occur at any stress level [30]. The plastic deformation of MGs is controlled by a cooperative atomic rearrangement termed as shear transformation zone (STZ) [38, 39]. STZ involving dozens of atoms is preferentially rooted in liquid-like zones. Thus, the structural rearrangement and change in the liquid-like zones during continuous irradiation can be identified from the activated state of the shear event. According to Hertzian elastic contact theory, the activation volume can be evaluated using statistical analysis. The cumulative distribution of strength (Fig. 6) can be expressed as [40]:

$$f = 1 - \exp\left[-\frac{kT\dot{\gamma}_0}{V^*(\mathrm{d}\tau/\mathrm{d}t)}\exp\left(-\frac{\Delta F^*}{kT}\right)\exp\left(\frac{\tau V^*}{kT}\right)\right] \quad (1)$$

where kT denotes the thermal energy, ΔF^* denotes the Helmholtz activation energy, and V^* is the activation volume of the shear event. V^* is the slope of the linear fit curves shown in the inset of Fig. 6, and its value is obtained by logarithmic conversion. The volume of an STZ (Ω) can be expressed by the following equation [41]:

$$\Omega = \frac{\tau_0}{6R_0G_0\gamma^2\xi(1-\tau/\tau_0)^{1/2}}V^* \quad (2)$$

where G_0 is the shear modulus at $T = 0$ K, and τ and τ_0 are the shear strengths at a finite temperature and $T = 0$ K.

As shown in Fig. 6(a), a clear trend can be observed in which the upper limit of τ_m continuously shifts to higher values as the fluence increased, indicating that yield was less likely to occur after ion irradiation. In addition, upon increasing the irradiation fluence, the volume of the STZ gradually decreased, as shown in the inset. Fig. 6(b) shows schematic depictions of the estimated changes in the STZ volume of MGs during irradiation at elevated temperature. The structural rearrangement of MGs can be determined by the cooperative shear motion of STZ, which inherently depends on the activation volume. Upon increasing the irradiation fluence at room temperature (RT), the liquid-like zone induced by irradiation increased in the MGs (Stage I). However, when increasing the irradiation time at 550°C, accompanied by thermal annealing, further increases in the liquid-like zone had to compete with liquid-like zone annihilation induced by crystallization during thermal annealing, which decreased the overall STZ volume (Stage II). Besides, τ_m follows the earlier trend of the nanohardness, supporting the widely-accepted theory of a direct link between elastic-plastic deformations in MGs. This suggests that the combination of ion irradiation and thermal annealing is a promising method to improve the mechanical properties by tuning the microstructure of MGs.

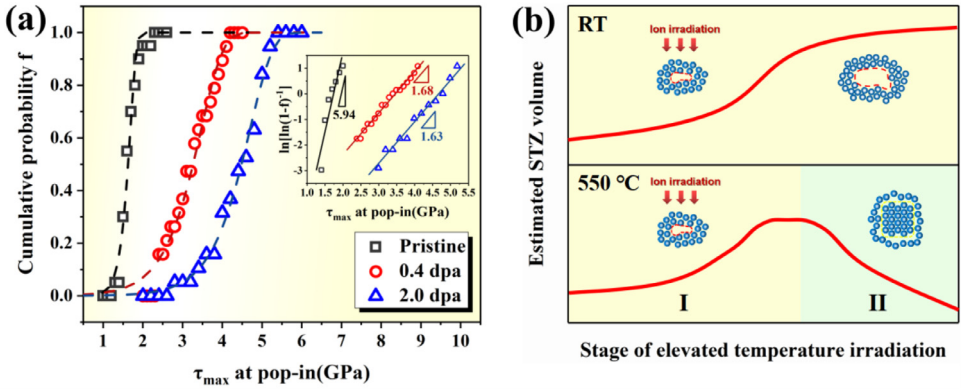

Fig. 6. (a) The cumulative distribution of the shear strength associated with the first pop-in event. The linear fits to the $\ln[\ln(1-f)^{-1}]$•kT versus τ_m curves are shown in the inset and were used to estimate the size of STZ in ZrTiHfCuBeNi MGs before and after irradiation. (b) Schematic representation of the estimated STZ volume variation in MGs during irradiation at elevated temperature.

4. Conclusions

The microstructure evolution and mechanical properties of ZrTiHfCuBeNi MGs after Xe^{29+} irradiation at 550 °C were investigated. The XRD results revealed that, unlike conventional thermal annealing, irradiation at elevated temperature resulted in crystallization and also formed complex intermetallic compounds. The irradiation-induced interstitial atoms may also enhance atomic migration and nanoparticle growth. Post-irradiation characterization using TEM analysis indicated that ion irradiation can also cause non-edge-on faulted dislocations in the formed nanoparticles due to irradiation-induced stress. The nanoindentation results revealed that the improved hardness, modulus, and plasticity in irradiated MGs were due to the formation of nanoparticles, as well as changes in the interatomic distances of the MGs. Moreover, the lagged first pop-in events after irradiation may be attributed to structural rearrangements and content changes in the liquid-like zone during continuous irradiation. The limit value τ_m showed a similar trend to the nanohardness at various fluences, which indicates a link between elastic-plastic deformations in MGs. These results suggest that combining ion irradiation with thermal annealing can improve the mechanical properties of an MG by tuning its microstructure.

Declaration of Competing Interest

(1) The authors declare that they have no known competing financial interests or personal relationships that could have appeared to influence the work reported in this paper.

(2) The authors declare the following financial interests/personal relationships which may be considered as potential competing interests.

Acknowledgements

This work was supported by the National Natural Science Foundation of China (Grant No. 51401028, No. 51271193, No. 11402277, No. 11790292) and the Strategic Priority Research Program of the Chinese Academy of Sciences (Grant No. XDB22040303). This work was also supported by the Innovation Program (237099000000170004).

Supplementary materials

Supplementary material associated with this article can be found, in the online version, at doi:10.1016/j.jnucmat.2020.152618.

References

[1] J. Luo, Y. Shi, Tensile fracture of metallic glasses via shear band cavitation, Acta Materialia 82 (2015) 483–490.
[2] H.F. Zhou, C. Zhong, Q.P. Cao, S.X. Qu, X.D. Wang, W. Yang, J.Z. Jiang, Non-localized deformation in metallic alloys with amorphous structure, Acta Materialia 68 (2014) 32–41.
[3] W.H. Wang, The elastic properties, elastic models and elastic perspectives of metallic glasses, Progress in Materials Science 57 (2012) 487–656.
[4] W.H. Wang, C. Dong, C.H. Shek, Bulk metallic glasses, Materials Science and Engineering: R: Reports 44 (2004) 45–89.
[5] A. Inoue, Stabilization of metallic supercooled liquid and bulk amorphous alloys, Acta Materialia 48 (2000) 279–306.
[6] W.H. Wang, The elastic properties, elastic models and elastic perspectives of metallic glasses, Progress in Materials Science 57 (2012) 487–656.
[7] J. Das, M.B. Tang, K.B. Kim, R. Theissmann, F. Baier, W.H. Wang, J. Eckert, Work-Hardenable, Ductile Bulk Metallic Glass. Physical Review Letters. 94 (2005) 205501.
[8] A.L. Greer, E. Ma, Bulk Metallic Glasses: At the Cutting Edge of Metals Research, MRS bulletin 32 (2007) 611–615.
[9] C.R. Cao, D.W. Ding, D.Q. Zhao, E. Axinte, H.Y. Bai, W.H. Wang, Correlation between glass transition temperature and melting temperature in metallic glasses, Materials & Design 60 (2014) 576–579.
[10] Y. Li, Y. Wei, K. Zhang, Y. Zhang, Y. Wang, W. Tang, B. Wei, Rejuvenation, embryonic shear bands and improved tensile plasticity of metallic glasses by nanosecond laser shock wave, Journal of Non-Crystalline Solids 513 (2019) 76–83.
[11] J. Antonaglia, W.J. Wright, X.J. Gu, R.R. Byer, T.C. Hufnagel, M. LeBlanc, J.T. Uhl, K.A. Dahmen, Bulk Metallic Glasses Deform via Slip Avalanches, Physical Review Letters 112 (2014) 155501.
[12] L. Tian, Y.Q. Cheng, Z.W.J. Li, C.C. Wang, X.D. Han, J. Sun, E. Ma, Approaching the ideal elastic limit of metallic glasses, Nature Communications 3 (2012) 609.
[13] O.V. Kuzmin, Y.T. Pei, C.Q. Chen, J.T.M. De Hosson, Intrinsic and extrinsic size effects in the deformation of metallic glass nanopillars, Acta Materialia 60 (2012) 889–898.
[14] K. Zhang, Z. Hu, F. Li, B. Wei, Viscous surface flow induced on Ti-based bulk metallic glass by heavy ion irradiation, Applied Surface Science 390 (2016) 941–945.
[15] J. Carter, E.G. Fu, G. Bassiri, B.M. Dvorak, N. David Theodore, G. Xie, D.A. Lucca, M. Martin, M. Hollander, X. Zhang, L. Shao, Effects of ion irradiation in metallic glasses, Nuclear Instruments and Methods in Physics Research Section B: Beam Interactions with Materials and Atoms 267 (2009) 1518–1521.
[16] E.G. Fu, J. Carter, M. Martin, G. Xie, X. Zhang, Y.Q. Wang, R. Littleton, L. Shao, Electron irradiation-induced structural transformation in metallic glasses, Scripta Materialia 61 (2009) 40–43.
[17] J. Carter, E.G. Fu, M. Martin, G. Xie, X. Zhang, Y.Q. Wang, D. Wijesundera, X.M. Wang, W.-K. Chu, L. Shao, Effects of Cu ion irradiation in $Cu_{50}Zr_{45}Ti_5$ metallic glass, Scripta Materialia 61 (2009) 265–268.
[18] W.D. Luo, B. Yang, G.L. Chen, Effect of Ar^+ ion irradiation on the microstructure and properties of Zr-Cu-Fe-Al bulk metallic glass, Scripta Materialia 64 (2011) 625–628.
[19] X. Zhang, X. Mei, Y. Wang, Y. Wang, J. Sun, The study of irradiation damage induced by proton in metallic glass $Ni_{62}Ta_{38}$ and metal W, Nuclear Instruments and Methods in Physics Research Section B: Beam Interactions with Materials and Atoms 436 (2018) 1–8.
[20] Y.X. Liang, J.L. Du, C. Xu, P.P. Wang, Z.Y. Hu, Y.H. Qiu, P. Wang, E.G. Fu, Roles of ion irradiation and thermal annealing in inducing crystallization in metallic glass, Intermetallics 114 (2019) 106608.
[21] L. Shao, E.G. Fu, L. Price, D. Chen, T. Chen, Y. Wang, G. Xie, D.A. Lucca, Sink property of metallic glass free surfaces, Scientific reports 5 (2015) 8877.

[22] Y. Wang, K. Zhang, Y.H. Feng, Y.S. Li, W.Q. Tang, Y.T. Zhang, B.C. Wei, Z. Hu, Excellent irradiation tolerance and mechanical behaviors in high-entropy metallic glasses, Journal of Nuclear Materials 527 (2019) 151785.
[23] Y. Wang, K. Zhang, Y.H. Feng, Y.S. Li, W.Q. Tang, Y.T. Zhang, B.C. Wei, Z. Hu, Mechanism of local hardening in metallic glass during He ion irradiation, Materialia 11 (2020) 100691.
[24] P. Gong, K.F. Yao, H.Y. Ding, Crystallization kinetics of TiZrHfCuNiBe high entropy bulk metallic glass, Materials Letters 156 (2015) 146–149.
[25] H.Y. Ding, K.F. Yao, High entropy $Ti_{20}Zr_{20}Cu_{20}Ni_{20}Be_{20}$ bulk metallic glass, Journal of Non-Crystalline Solids 364 (2013) 9–12.
[26] M. Yang, X.J. Liu, H. Ruan, Y. Wu, H. Wang, Z. Lu, High thermal stability and sluggish crystallization kinetics of high-entropy bulk metallic glasses, Journal of Applied Physics 119 (2016) 245112.
[27] .Y.H. Qiu, C. Xu, E.G. Fu, P.P. Wang, J.L. Du, Z.Y. Hu, X.Q. Yan, X.Z. Cao, Y.G. Wang, L. Shao, Mechanisms for the free volume tuning the mechanical properties of MG through ion irradiation, Intermetallics 101 (2018) 173–178.
[28] D. Chen, Y. Tong, J. Wang, B. Han, Y. Zhao, F. He, J.J. Kai, Microstructural response of He^+ irradiated $FeCoNiCrTi_{0.2}$ high-entropy alloy, Journal of Nuclear Materials 510 (2018) 187–192.
[29] G.K. Liao, Z.L. Long, M.S.Z. Zhao, L. Peng, W. Chai, Z.H. Ping, Nanoindentation study on the characteristic of shear transformation zone in a Pd-based bulk metallic glass during serrated flow, Physica B: Condensed Matter 534 (2018) 163–168.
[30] Y. Li, K. Zhang, Y. Wang, W. Tang, Y. Zhang, B. Wei, Z. Hu, Abnormal softening of Ti-metallic glasses during nanosecond laser shock peening, Materials Science and Engineering: A 773 (2020) 138844.
[31] C.A. Schuh, T.G. Nieh, A nanoindentation study of serrated flow in bulk metallic glasses, Acta Materialia 51 (2003) 87–99.
[32] W.J. Wright, R. Saha, W.D. Nix, Deformation Mechanisms of the $Zr_{40}Ti_{14}Ni_{10}Cu_{12}Be_{24}$ Bulk Metallic Glass, Materials Transactions JIM 42 (2001) 642–649.
[33] W.J. Wright, R.B. Schwarz, W.D. Nix, Localized heating during serrated plastic flow in bulk metallic glasses, Materials Science and Engineering: A 319-321 (2001) 229–232.
[34] D. Wang, X. Lu, Y. Deng, D. Wan, Z. Li, A. Barnoush, Effect of hydrogen-induced surface steps on the nanomechanical behavior of a CoCrFeMnNi high-entropy alloy revealed by in-situ electrochemical nanoindentation, Intermetallics 114 (2019) 106605.
[35] K.L. Johnson, Contact Mechanics, Cambridge University Press, Cambridge, 1987.
[36] A. Barnoush, H. Vehoff, Recent developments in the study of hydrogen embrittlement: Hydrogen effect on dislocation nucleation, Acta Materialia 58 (2010) 5274–5285.
[37] W.W. Gerberich, J.C. Nelson, E.T. Lilleodden, P. Anderson, J.T. Wyrobek, Indentation induced dislocation nucleation: The initial yield point, Acta Materialia 44 (1996) 3585–3598.
[38] W.L. Johnson, K. Samwer, A Universal Criterion for Plastic Yielding of Metallic Glasses with a $(T/T_g)^{2/3}$ Temperature Dependence, Physical Review Letters 95 (2005) 195501.
[39] Yu.I. Golovin, V.I. Ivolgin, V.A. Khonik, K. Kitagawa, A.I. Tyurin, Serrated plastic flow during nanoindentation of a bulk metallic glass, Scripta Materialia 45 (2001) 947–952.
[40] C.A. Schuh, A.C. Lund, Application of nucleation theory to the rate dependence of incipient plasticity during nanoindentation, Journal of Materials Research 19 (2004) 2152–2158.
[41] I.C. Choi, Y. Zhao, B.G. Yoo, Y.J. Kim, J.Y. Suh, U. Ramamurty, J. Jang, Estimation of the shear transformation zone size in a bulk metallic glass through statistical analysis of the first pop-in stresses during spherical nanoindentation, Scripta Materialia 66 (2012) 923–926.